ELSEVIER

Journal of Power Sources 86 (2000) 383–389

JOURNAL OF POWER SOURCES

www.elsevier.com/locate/jpowsour

Preparation of Ni–YSZ composite materials for solid oxide fuel cell anodes by the gel-precipitation method

Marjan Marinšek *, Klementina Zupan, Jadran Maček

Faculty of Chemistry and Chemical Technology, University of Ljubljana, Aškerčeva 5, 1000 Ljubljana, Slovenia

Abstract

Nickel oxide–yttria stabilized zirconia powder mixtures (Ni–YSZ) were prepared by the gel-precipitation method from aqueous or methanol solutions of the corresponding chlorides. The sinterability of the powder mixtures and hence their appropriateness as anodic material in solid oxide fuel cell technology (SOFC) is affected both by the history of the powder preparation and its composition. Relative densities of greater than 97% of theoretical of the mixed NiO–YSZ powder were achieved at sintering temperatures as low as 1300°C. In sintered samples, both NiO and YSZ, composites could be prepared as continuous phases if the chemical composition of the prepared powder mixture were carefully controlled. The continuity of the YSZ and Ni phases was preserved after reduction as well. If the ceramic YSZ phase was prepared as a continuous rigid framework there was practically no shrinkage of the sintered body during reduction, but the reduced matrices became porous and the relative densities were lowered. The microstructural and electrical properties of Ni–YSZ cermets, where the Ni content in the YSZ matrix is close to 35 vol.%, showed that the materials are appropriate for SOFC anode preparation.

Keywords: Ni–YSZ; Cermet; Solid oxide fuel cell anode; Gel-precipitation

1. Introduction

The interest in utilizing fuel cells as an energy source system has grown substantially over recent years [1]. However, all the problems connected with the techniques of material preparation and fuel cell stack fabrication have not yet been solved. Among other characteristics the three requirements of prime importance for anode materials are good electrical properties, an appropriate microstructure of the anode composites and compatibility with other fuel cell components [2,3]. Anode composite materials are presently manufactured utilizing the mechanical mixing method, where separately prepared nickel oxide (NiO) and yttria stabilized zirconia (YSZ) powders are subsequently subjected to homogenization and sintering to form a Ni–YSZ cermet [4]. However, a problem with mechanical mixing can occur due to separation of NiO and YSZ particles, resulting in a nonuniform distribution of Ni in the anode material if the homogenization and grinding are not performed correctly. Thus, recent studies on Ni–YSZ cermet preparation were focused toward using preparation techniques that would assure a very uniform distribution of Ni particles in the ceramic matrix, either by controlling the Ni and YSZ particle size distribution [5] or the sintering temperature [6]. These requirements can be provided by using the gel-precipitation method and subsequent sintering of the intermediates obtained [7]. The technique of simultaneous gel-precipitation enables mixing of precursors already in the starting solution, resulting in a gel mixture with a high degree of homogeneity, where one phase dominance is very small [8]. By subsequent heat treatment of the prepared green composite materials, different anode microstructures can be obtained. Additionally, a range of electrode characteristics such as porosity, nickel particle distribution, grain size and particle to particle contact may result from these differing electrode microstructural properties [9].

In all processes where powder particles are involved in the green body forming technique, the final processing step requires sintering. The sintering process provides bonds between particles and continuity of the different phases in the composite material [10]. However, the electrode layer should be porous and permeable enough to provide diffusion both of the fuel gas supply to and the removal of the

* Corresponding author.

0378-7753/00/$ - see front matter
PII: S0378-7753(99)00425-5

gaseous reaction products from the electrode/electrolyte interface [11]. The enhanced contact area between the electrocatalyst and the ionic conductor results in rather low overvoltages and consequent high current densities, which improve the overall cell performance.

The objective of the present study was to determine the effect of several processing variables of sintering on the powder characteristics and densification, as well as on the microstructure of the fired body. The influence of the precursor chemical composition on the characteristics of the Ni–YSZ cermet after complete thermal treatment was studied. Some electrical electrode performance as a function of microstructural and chemical properties was conducted and discussed.

2. Experimental method

Zirconium, yttrium and nickel were precipitated from aqueous (samples B, C, D, E, F and I) or methanol solutions by the addition of a twofold stoichiometric amount of water (samples A, G, H, J and K) by the gel-coprecipitation method. Samples B, C, D and E were prepared at 97°C, while samples F, I and J were prepared at 75°C. Samples A, G, H and K were prepared at room temperature (Table 1). Elevated temperatures and different solvents were used in the starting material preparation path to achieve some improvement in the control of the hydrolysis reactions and thus the yield of nickel hydroxide in the mixed gel.

The starting solutions of the metal chlorides were prepared by dissolving 38 g of $NiCl_2 \cdot 6H_2O$ (Kemika Zagreb, p.a.) and the corresponding amounts of $ZrCl_4$ (Fluka, assay > 98%) and Y_2O_3 (Aldrich Chemical, 99.99%; dissolved in HCl) in 400 ml of solvent to achieve the desired mixed gel composition. The amount of yttrium precursor in the starting reaction mixture was selected so that the final molar ratio of Y_2O_3 to ZrO_2 was 10:90 (10 mol% YSZ). The hydrolysis reaction was initiated by the introduction of gaseous ammonia (flow rate 3.88 l/h, final pH value 8). The product was filtered, washed with distilled water until no reaction for chloride ions was observed ($AgNO_3$ test) and dried for 6 h at 120°C. The dried samples were milled in a ball mill, calcined at 950°C for 2 h, pressed into tablets (6 mm in diameter, pressed under 49 MPa or 500 kg/cm^2) and then subjected to further thermal treatment (sintering at 1300°C and temperature programmed reduction (TPR) in a dynamic atmosphere of 4 vol.% hydrogen and 96 vol.% argon at 1000°C for 2 h).

Table 1
Sample preparation

Sample	Initial mol ratio Zr^{4+}:Y^{3+}:Ni^{2+}	Preparation temperature (°C)	Solvent	Theoretical composition (wt.% of Ni in Ni–YSZ)
A	(pure NiO)	97	water	100
B	4.50:1.00:252.60	97	water	95.00
C	4.50:1.00:113.03	97	water	89.48
D	4.50:1.00:57.01	97	water	81.09
E	4.50:1.00:40.72	97	water	75.39
F	4.50:1.00:38.31	97	water	74.24
G	4.48:1.00:81.12	10	methanol	85.96
H	4.50:1.00:40.72	75	methanol	75.39
I	4.50:1.00:40.72	75	water	75.39
J	4.64:1.00:25.70	10	methanol	65.41
K	(pure YSZ)	10	methanol	0

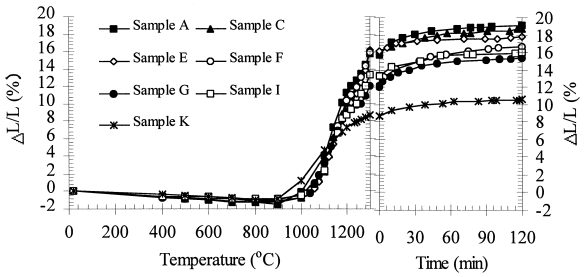

Fig. 1. Dimensional changes of samples A to K during firing. The densification of NiO, as well as the densification of composite materials, occurs in the rapid region of densification at two different shrinkage rates.

The reaction medium and preparation conditions have a marked influence on the product characteristics. These differences in process conditions can lead to substantial variations in the end products composition, as in the case where the initial ratio of the reactants was the same. Higher preparation temperature and the use of methanol as a solvation medium raise the amount of precipitated $Ni(OH)_2$ and consequently the amount of Ni in the final composite [12].

The amount of nickel in the samples was determined by a volumetric method. The particle size distribution of the calcined precipitates was determined by laser beam diffraction (Fritsh Analysette 22). Calcined powders for particle size distribution measurements were dispersed in 1% NaCl aqueous solution. The microstructure of the as-sintered and polished samples as well as transverse cross-sections were examined by scanning electron microscopy and energy-dispersive X-ray analysis (SEM-EDX, Jeol 5800). Thermal analysis (TG, DTA, Netzsch 409) was used for further characterization of the samples. Dimensional changes during heating were measured by a heating microscope by heating the samples up to 1300°C with a heating rate of 10 K/min and then thermostatting them at 1300°C for 120 min. Calculations of relative densities of fired samples were made on the presumption that NiO or Ni and YSZ do not form any chemical compound or solid solution.

AC impedance measurements of the thermally treated samples were carried out using an impedance analyzer (Hewlett Packard 4284A) over the frequency range from 20 Hz to 1 MHz at 1000°C in a dynamic reductive atmosphere (4 vol.% H_2 and 96 vol.% Ar). Prior to the

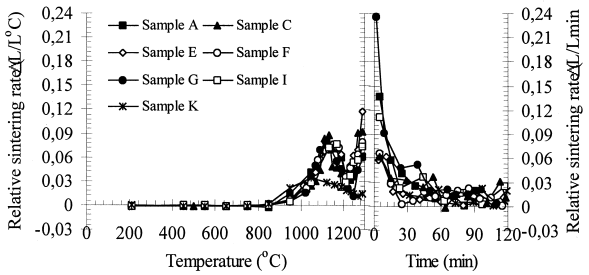

Fig. 2. Relation between the relative rate of sintering and the temperature of NiO–YSZ cermets.

electrical measurements, all samples were painted with platinum paste and held in a Pt grid from both sides.

3. Results and discussion

The cermet anode has a rather complex structure because the electronic and the ionic paths must be separately supported by nickel and yttria-stabilized zirconia particle networks, respectively. Furthermore, the anode layer must remain porous (approximately 30% by volume) and permeable to allow the transport of reactant and evolved gases during the cell operation [13]. Such a structure with the desired microstructual and electrical properties, as well as long term stability performance, dictates a rather precise anode preparation route. The crucial step in the preparation of the anode is the use of precursor powders with the appropriate composition and careful application of predetermined sintering conditions.

The sintering behaviour of the NiO–YSZ composites with different chemical compositions was determined by a heating microscope. The shrinkage curves and the curves of relative shrinkage rates are depicted in Figs. 1 and 2, respectively. Three different domains may be identified. The samples exhibited normal volume expansion in the 20–900°C temperature range. Fast shrinkage was observed in all samples at temperatures slightly above 1100°C, except in the case of sample K (pure YSZ), where accelerated shrinkage began at temperatures close to 1000°C. A decrease in the shrinkage rate was found in the temperature range between 1200° and 1250°C. A second domain of fast densification was noticed when the temperature exceeded 1250°C, whereas after the stabilisation of the temperature at 1300°C, the densification rate of the samples drastically decreased.

The sintering of pure YSZ begins at slightly lower temperatures than the sintering of NiO–YSZ samples. However, NiO–YSZ samples densify much faster at temperatures above 1100°C in comparison with the densification of YSZ. Consequently, precursors with a higher amount of NiO reach higher theoretical densities after thermal treatment (Table 2).

The two different relative shrinkage rates in the sintering of composites are related to the chemical composition of the material and the particle packing in the green body. According to Fig. 2 all composites that contain NiO should sinter via two different sintering processes. Because YSZ and NiO do not undergo any chemical reactions, we assumed that variation in the sintering rates could be a consequence of either some polydispersion effects of the starting powder precursors, or some possible physical transitions during sintering such as recrystallization or melting. To distinguish between these two phenomena we submitted a composite to TG–DTA measurement and looked for possible mass or heat transfer reactions (Fig. 3).

According to the TG–DTA curves of the calcined samples A and E (Fig. 3) no heat transfer reactions, e.g., phase recrystalization, took place during the analysis. Sample A exhibits an almost constant mass during heating up to 1400°C, while when heated to temperatures higher than 1000°C, there is a slight mass loss of 0.4% in the case of sample E. However, no clear and stepwise chemical or physical change in the sample is evident.

A comparison of the relative shrinkage (Table 2), which increases with the amount of NiO in the composite material, indicates that NiO phase promotes shrinkage of the

Table 2
Density change during sintering as a function of NiO content in the precursors

Sample	Wt.% of NiO in the sample	ρ_{green} (g/cm^3)	Relative ρ_{green} (%)	$\rho_{sintered}$ (g/cm^3)	Relative $\rho_{sintered}$ (%)	$\Delta L/L$ (%)
A	100 (pure NiO)	3.41	51.12	6.45	96.64	19.13
B	93.66	3.35	50.77	6.31	95.67	18.79
C	85.95	3.21	49.31	6.37	96.83	18.73
D	79.53	3.25	50.47	6.22	96.56	18.16
E	60.83	3.37	55.05	6.06	97.22	17.77
F	69.55	3.31	52.29	6.18	97.64	17.08
G	48.11	3.36	55.09	5.61	91.90	16.64
H	31.56	3.21	52.73	5.28	90.89	15.32
I	22.42	3.02	59.83	5.10	88.06	16.05
J	18.41	3.12	54.05	5.21	89.91	15.72
K	0 (pure YSZ)	2.52	45.27	3.94	63.31	10.58

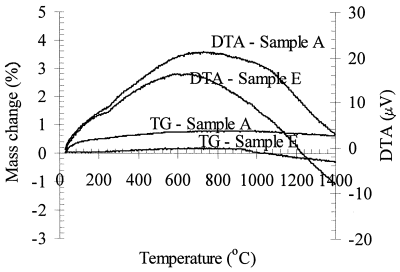

Fig. 3. TG–DTA pattern of samples A and E.

fired composites. Relative sintered densities decrease with the decline of the amount of NiO in the fired precursor. Maximum sintered densities, ≈97% and ≈96% of the theoretical density, and highest relative shrinkages were obtained in the case of sample A (pure NiO) and composites richest in NiO, respectively. Additionally, relatively high shrinkage of the fired samples (except for sample K) and the high amount of NiO result in a rather small degree of porosity of the fired samples (Fig. 4).

The sintering route and some differences in the microstructure of the sintered samples can also be interpreted with respect to the mean particle sizes of the powder precursors (Fig. 6). Although there are still some drastic changes in particle to particle bonding occurring during thermal treatment of the samples, chemical composition and some morphological characteristics of the starting precursors to a large degree determine the microstructure of the sintered composites. According to Fig. 5 NiO and YSZ consist of small particles called primary aggregates. The frequency particle size distribution of NiO, YSZ and

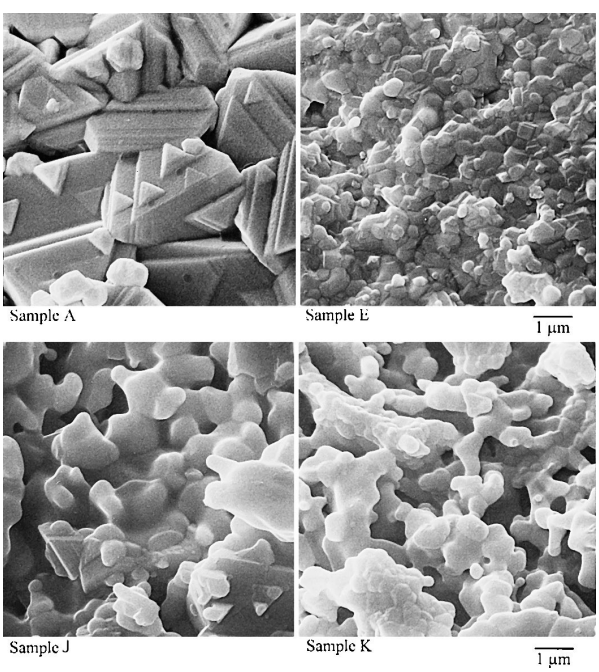

Fig. 4. Microstructures of the cross sections of some NiO–YSZ composites after sintering.

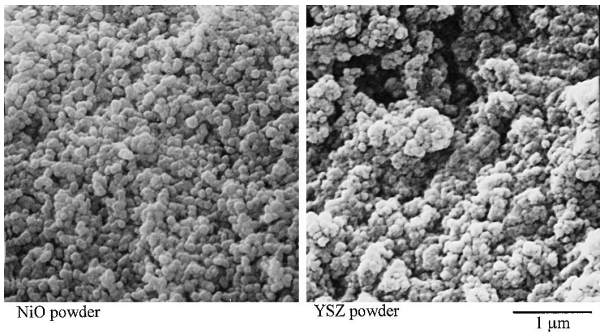

Fig. 5. SEM images of NiO and YSZ powders after calcination.

mixed powder precursors in Fig. 6 reveals that these primary aggregates, which are formed during gel-precipitation and subsequent calcination, merge forming larger agglomerates of various mean sizes (up to a few micrometers). As samples are prepared from aqueous or methanol solutions at rather different temperatures, the particle size distributions of powder precursors in the green state are rather different. When more or less agglomerated precursors are sintered, the composite starts to densify because of particle to particle bonding. The two different sintering regions indicate that there should be two different sintering processes. The first increase in the shrinkage rate is connected with particle sintering inside the agglomerate (intra-agglomerate sintering). Inter-agglomerate sintering starts at higher temperatures in the second domain of fast densification. It can be calculated that at a sintering temperature of 1300°C both intra- and inter-agglomerate sintering of NiO occurred resulting in rather high relative sintered densities, while inter-agglomerate sintering of the YSZ phase is not entirely completed.

On the other hand, the formation of smaller and less agglomerated mixed powder precursors in comparison to the formation of mixed precursors of larger mean particle size results in smaller dominance of single-phase domains where only NiO or YSZ phase is present. Single-phase domains are preserved, or slightly enlarged during sintering. However, the main purpose of composite material sintering is to ensure good particle-to-particle bonding and the continuity of NiO and YSZ phases throughout the sample.

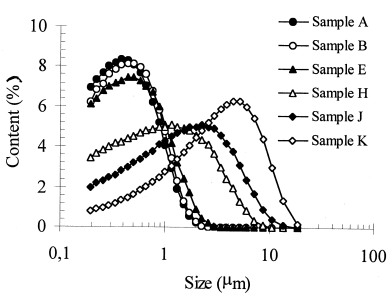

Fig. 6. Frequency particle size distribution of the calcined powder precursors.

The continuity of the YSZ phase was estimated by measuring the dimensional changes in the sintered tablets during reduction of NiO to metallic Ni (Table 3). If the YSZ particles, after sintering, form a three-dimensional continuous network, there should be no volume contraction of the composite tablet. On the contrary, if sintering does not assure a YSZ net structure rigid enough to withstand the contraction pressures, which occur during the reduction of NiO to Ni, the composite will shrink because of nickel sintering. As NiO and YSZ do not form solid solutions, NiO grains should sinter separately and if the amount of NiO in the composite is high enough, it should create a continuous phase as well. According to the results in Table 3 good contact between YSZ particles and NiO particles respectively was achieved during sintering at 1300°C in all cases where Ni content in the final composite did not exceed 64 wt.%. A higher amount of Ni in the composite (above 75 wt.%) isolates the YSZ phase into separate islands, leading to excessive Ni sintering.

The growth of Ni grains and thus, degradation of the reaction surface area, is the fundamental problem during long-term operation of an SOFC cell stack, if the YSZ matrix in the anode material does not form a rigid framework. Micrographic investigations were performed on reduced and polished samples (Fig. 7). The micrograph of sample E exhibits a good distribution of Ni particles inside the YSZ matrix (Ni particles are represented by fine spheres captured inside the matrix). Fine Ni particles in the micro- or submicrometer range are distributed uniformly with fine pores surrounding them. Because the sintered nonreduced samples are rather dense, these pores seem to be formed by volume contraction caused by the reduction of NiO particles. Volume reduction during TPR results in the formation of very fine pores adjacent to the Ni particles. This increases the triple-phase boundary area between fuel gas, iono-conductor (YSZ) and the electrocatalyst Ni, if the material were to be used in an SOFC stack. This triple-phase boundary is less pronounced after prolonged thermal treatment at elevated temperatures. However, although the YSZ–Ni–fuel contact area is large due to such particle-to-particle bonding, which is not beneficial, it still contributes to the composite's long-term stability and promotes phase continuity.

Table 3
Material densification during TPR as a function of Ni content in the composite

Sample	Wt.% of Ni in the composite	$\rho_{\text{after reduction}}$ (g/cm^3)	Relative $\rho_{\text{after reduction}}$ (%)	Composite volume change during reduction (%)
A	99.56	7.19	80.92	−20.50
B	92.07	6.67	77.26	−11.23
C	82.78	5.33	64.03	−4.93
D	75.22	5.86	72.61	−2.52
E	54.06	5.50	74.82	0
F	63.83	5.63	73.26	0
G	42.11	5.34	76.82	0
H	26.06	4.98	77.56	0
I	18.31	4.88	79.29	0
J	14.26	4.90	81.39	0
K	0	3.94	63.31	0

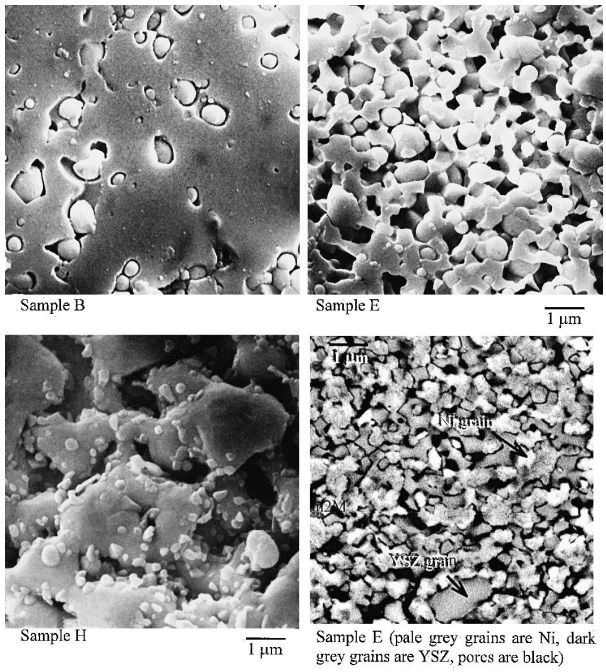

Fig. 7. Microstructures of polished samples B, E and H after TPR and a backscattered electron image of reduced and polished sample E.

The most apparent difference in the microstructure between these samples is the pore and phase distribution throughout the composite. Ni and YSZ grains in sample E (pale grey and dark grey regions in the BEI image, respectively) are in the micrometre range and both phases are continuous. The microstructure of sample B reveals an excessive Ni grain growth, while in the case of sample H, Ni grains are isolated and thus do not represent a continuous phase.

Nickel phase is added to the composite material to serve as an electrocatalyst for hydrogen oxidation and to provide the anode with an electric conductivity as high as possible. To satisfy these two conditions, the Ni phase must become continuous during the preparation route. The easiest way to

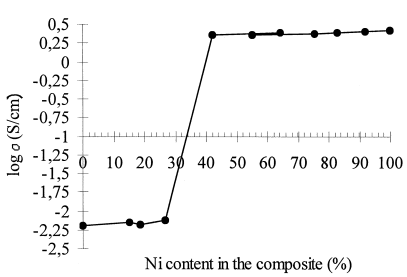

Fig. 8. Effect of Ni content on the specific electrical conductivity of Ni–YSZ composites at 1000°C.

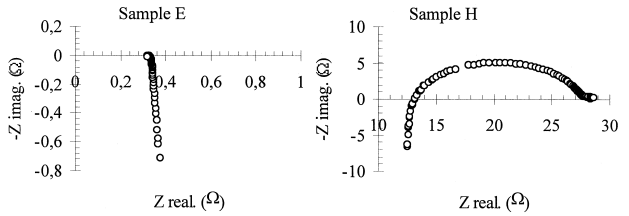

Fig. 9. Typical impedance spectra of electronic and ionic composite conductors measured in an Ar–4 vol.% H_2 atmosphere at 1000°C.

verify the continuity of the nickel phase is to measure the electrical performance of the composite, which depends mainly on the nickel distribution throughout the sample (Fig. 8).

The electrical behaviour of Ni–YSZ samples can be explained by percolation theory [14]. Ni grains can act as a continuous metallic medium allowing the electrons to migrate throughout the material. This requires a threshold value of Ni content (30 vol.% is considered the boundary between an essentially ionic and essentially electronic conduction) [14–16] and an appropriate microstructure which depends on composite morphology (Fig. 7).

According to the impedance measurements, all samples from A to G are electrically conducting. The relatively high value of electrical conductivity in the case of samples A to G at 1000°C in a reducing atmosphere (≈ 0.4 S/cm which is very close to the conductivity of pure metallic nickel) proves that the nickel phase must be continuous. The impedance spectrum of an electronic conductor is reduced to a single dot (Fig. 9). No capacitive elements were observed when varying the frequency through the chosen range. The vertical part below the real axis is probably due to some inductive elements in the experimental set-up. In contrast, the continuity of the nickel phase is not preserved if the nickel content in the composite material is reduced to 26 wt.% or below. The discontinuity of nickel phase is clearly evident in the microstructure of sample H (Fig. 7). In this case, nickel particles form small nickel islands that are not in contact with the neighbouring ones. The electrical conductivity of Ni–YSZ cermets with low nickel content (≈ 0.035 S/cm) is similar to the electrical conductivity of the pure YSZ matrix. The impedance spectra of samples where the nickel content in the composite is below 26 wt.% show depressed overlapped arcs, which could be associated with at least two capacitive loops (Fig. 9, sample H). The impedance behaviour has been measured for all samples and it was shown that ionic conductivity is dominant in the case of samples H to K.

Cermets with a relatively low Ni content may have long-term stability and well-developed microstructure but from the electrochemical point of view they are not suitable as anode material in an SOFC. On the other hand, Ni–YSZ composites with a Ni content high enough to initiate material shrinkage during the TPR do not meet the requirement of long-term stability microstructure and have a very undeveloped Ni–YSZ–fuel triple-phase boundary. The amount of Ni in the Ni–YSZ composite needed to prevent anode microstructure degradation and leading to dominant electronic conductivity through the material must stay within 42 to 54 wt.%. Such composites could be used in the cell stack preparation route as anode material.

4. Conclusion

The gel-precipitation method is an attractive method for Ni–YSZ cermet preparation as it enables relatively good mixing of the metal and ceramic phases at the level of a very small single-phase dominance. In this way, stable Ni–YSZ composite materials, resistant toward elevated temperatures with respect to their chemical and mechanical properties, can be prepared with continuous ceramic and metal phases. The continuity of the ceramic YSZ rigid framework is assumed because there is practically no shrinkage of the composites during the reduction of NiO to Ni. The continuity of the YSZ phase also contributes to the continuity of an ionic path during anode performance and, thus, also to the enlargement of the reaction zone. The indication of a continuous nickel phase throughout the samples is their high electronic conductivity. Drastic changes in values were obtained with increase of nickel from 30% to 40% in the composite material, as expected from percolation theory. Conductivity becomes electronic only above 42% (approximately 31 vol.%) of nickel, meaning that above this the nickel phase must be continuous. To enhance electronic conductivity, the cermet should have a Ni concentration higher than 35 vol.%.

References

[1] S.P.S. Badwal, K. Foger, Solid oxide fuel cell review, Ceram. Int. 22 (1996) 257–265.
[2] N.Q. Minh, Ceramic fuel cells, J. Am. Ceram. Soc. 76 (3) (1993) 563–588.
[3] N.Q. Minh, High temperature fuel cells. Part 2: The solid oxide cell, CHEMTECH 2 (1991) 120–126.
[4] J. Larminie, Fuel cells come down to earth, IEE Rev. 42 (3) (1996) 106–109.
[5] S. Murakami, Y. Akiyama, N. Ishida, T. Yasuo, T. Saito, N. Furukawa, Development of a solid oxide fuel cell with composite anodes, in: F. Grosz, P. Zegers, S.C. Singhal, O. Yamamoto (Eds.), Solid Oxide Fuel Cells, Proc. 2nd Int. Symp., Commission of the European Communities, Athens, Greece, 1991, pp. 105–112.
[6] T. Shirakawa, S. Matsuda, A. Fukushima, Characterization of NiO/YSZ electrode by temperature-programmed reduction, in: S.C. Singhal, H. Iwahara (Eds.), Solid Oxide Fuel Cells, Proc. 3rd Int. Symp., Electrochemical Society, Pennington, NJ, 1993, pp. 464–472.
[7] M. Valigi, D. Gazzoli, R. Dragone, M. Gherardi, G. Minelli, Nickel oxide–zirconium oxide: Ni^{2+} incorporation and its influence on the phase transition and sintering of zirconia, J. Mater. Sci. 5 (1) (1995) 183–189.
[8] W. Johnson Jr., Sol–gel processing of ceramics and glass, Ceram. Bull. 64 (12) (1985) 1597–1602.

[9] T. Kawada, N. Sakai, H. Yokokawa, M. Dokiya, M. Mori, T. Iwata, Characteristics of slurry-coated nickel zirconia cermet anodes for solid oxide fuel cells, J. Electrochem. Soc. 137 (10) (1990) 3042–3047.

[10] M. Mogensen, S. Primdahl, J.T. Rheinlander, Composite electrodes: morphology and properties, Advanced Fuel Cells Programme Annex II, Modelling and Evaluation of Advanced Solid Oxide Fuel Cells, 7th SOFC Workshop, Norway, 1995, pp. 53–57.

[11] E. Fendler, R. Henne, M. Lang, SOFC anode layers with controlled porosity by vacuum plasma spraying, in: Ulf Bossel, Druckerei J. Kinzel, (Eds.), Proc. 1st European Solid Oxide Fuel Cell Forum, Vol. 2, Göttingen, Lucerne Switzerland, 1994, pp. 629–631.

[12] M. Marinšek, PhD thesis, University of Ljubljana, Faculty of Chemistry and Chemical Technology, Ljubljana, 1998, pp. 109–121.

[13] L.J. Gauckler, K. Sasaki, A. Mitterdorfer, M. Gödickemeier, P. Bohac, Processing of SOFC Ceramic Components, in: Ulf Bossel (Ed.), Proc. of 1st European Solid Oxide Fuel Cell Forum, Vol. 2, Druckerei J. Kinzel, Göttingen, Lucerne, Switzerland, 1994, 545–566.

[14] E. Ivers-Tiffee, W. Wersing, M. Schiel, H. Greiner, Ceramic and metallic components for planar SOFC, Ber. Bunsen-Ges. 94 (1990) 978–981.

[15] T. Kawada, N. Sakai, H. Yokokawa, M. Dokiya, M. Mori, T. Iwata, Structure and polarization characteristics of solid oxide fuel cell anodes, Solid State Ionics 40–41 (1990) 402–406.

[16] D.W. Dees, T.D. Claar, T.E. Easler, D.C. Fee, F.C. Mrazek, Conductivity of porous Ni–ZrO_2–Y_2O_3 cermets, J. Electrochem. Soc. 134 (1987) 2141–2146.